FFI RAPPORT

STATIC MAGNETIC DIPOLE DETECTION – Generalized matched filtering to Anderson functions

OTNES Roald

FFI/RAPPORT-2006/03373

STATIC MAGNETIC DIPOLE DETECTION – Generalized matched filtering to Anderson functions

OTNES Roald

FFI/RAPPORT-2006/03373

FORSVARETS FORSKNINGSINSTITUTT
Norwegian Defence Research Establishment
P O Box 25, NO-2027 Kjeller, Norway

FORSVARETS FORSKNINGSINSTITUTT(FFI)
Norwegian Defence Research Establishment

P O BOX 25
NO-2027 KJELLER, NORWAY

UNCLASSIFIED

SECURITY CLASSIFICATION OF THIS PAGE
(when data entered)

REPORT DOCUMENTATION PAGE

1) PUBL/REPORT NUMBER	2) SECURITY CLASSIFICATION	3) NUMBER OF PAGES
FFI/RAPPORT-2006/03373	UNCLASSIFIED	33
1a) PROJECT REFERENCE	**2a) DECLASSIFICATION/DOWNGRADING SCHEDULE**	
FFI-IV/886/914	-	

4) TITLE

STATIC MAGNETIC DIPOLE DETECTION – Generalized matched filtering to Anderson functions

5) NAMES OF AUTHOR(S) IN FULL (surname first)

OTNES Roald

6) DISTRIBUTION STATEMENT

Approved for public release. Distribution unlimited. (Offentlig tilgjengelig)

7) INDEXING TERMS

IN ENGLISH	IN NORWEGIAN
a) Magnetic detection	a) Magnetisk deteksjon
b) Signal Processing	b) Signalbehandling
c) Linear Prediction	c) Lineær prediksjon
d) Matched filter	d) Tilpasset filter
e) Anderson functions	e) Anderson-funksjoner

THESAURUS REFERENCE:

8) ABSTRACT

We propose a method for combined noise suppression and target detection for 3-axial magnetometer measurements. Vector linear prediction is used to whiten the noise, and matched filters are used for detection. In a case study, we are able to extract a decision variable with an SNR of 20 dB from an input signal where the amplitude of the target is similar to the noise amplitude. A block-based adaptive procedure for use on a buffered stream of input data is also proposed. Good detection performance is achieved on real data, with a detection delay of 85 seconds.

9) DATE	AUTHORIZED BY	POSITION
2006-10-30	This page only Tor Knudsen	Director of Research

ISBN 978-82-464-1095-1

FFI-B-22-1982

UNCLASSIFIED

SECURITY CLASSIFICATION OF THIS PAGE
(when data entered)

CONTENTS

page

STATIC MAGNETIC DIPOLE DETECTION

Generalized matched filtering to Anderson functions

1 EXECUTIVE SUMMARY

Underwater sensor networks for area surveillance has recently become a topic of interest in the international underwater (defence) research community, also being studied at FFI. Such a sensor network will typically employ sensor nodes with multiple sensor types, in particular static magnetic sensors and passive acoustic sensors.

For underwater sensor networks, detection ranges should be as large as possible in order to minimize the required number of sensors to cover a given area. This contrasts the most common historical use of underwater static magnetic detection as triggering mechanism for sea mines, where the detection range should not be larger than the damage radius of the mine.

This report deals with detection of static magnetic signals, performed in combination with noise suppression. We address the case where measurements from only a single 3-axial magnetometer are available. The main noise source in this case is fluctuations in the geomagnetic field.

It is well known that geomagnetic fluctuations can be suppressed by subtracting off a reference measurement made some distance away. In an underwater sensor network, we do however not expect to have the capacity to communicate raw measurement data between sensors, and hence the goal of the present work is to autonomously achieve the best possible detection performance with the measurement data available at a single sensor location.

We propose a method where vector linear prediction is used to whiten the noise, and matched filters are used for detection. The filters are matched to the result of passing the Anderson functions through the noise whitening filters.

In a case study, we are able to extract a decision variable with an SNR of 20 dB from an input signal where the amplitude of the target signal is similar to the noise amplitude. This directly implies increased detection range, as a gain of 20 dB corresponds to increasing the detection range by a factor 2.15.

The performance of the algorithm on scalar signals (e.g., total-field magnetometers) is clearly inferior to its performance when using 3-axial magnetometers.

A block-based adaptive procedure for use on a buffered stream of input data is also proposed. Good detection performance is achieved on real data, with a detection delay of 85 seconds. We plan to use this algorithm at sea trials in the near future, for real-time on-site assessment of the detection performance.

2 INTRODUCTION

The work described in this report is related to the projects 886 NIMSES (Network Integrated Maritime Sensor and Effector Systems) and 1039 “NbF under vann” (Underwater network-centric defence) at FFI, and to the NGAS JRP (Next Generation Autonomous Sensors, Joint Research Project) between NATO URC, DRDC-Atlantic (CA), ONR/SPAWAR (US), and FFI.

The topic of this report is detection of so-called “static magnetic” signals, i.e., the time-varying local perturbation (magnetic anomaly) in the Earth’s magnetic field when an object with a permanent and/or induced magnetic moment is passing by. Using a magnetometer to sense the magnetic field in a particular location, this can be observed as perturbations around a large DC component corresponding to the Earth’s magnetic field. Magnetometers are either tri-axial (measuring the vector components of the magnetic field) or scalar (measuring the absolute value or L_2-norm of the magnetic field vector).

Underwater magnetic detection has historically been used as triggering mechanism for sea mines, where the detection range should not be larger than the damage radius of the mine. More recently, underwater sensor networks for area surveillance has become a topic of interest. For such systems, detection ranges should be as large as possible in order to minimize the required number of sensors to cover a given area.

Underwater magnetometer measurements exhibit the following noise sources:

- Instrumentation noise
- Geomagnetic fluctuations (variations in the Earth’s magnetic field)
- Motion-induced noise (when a tri-axial sensor is rotated the apparent components of the Earth’s magnetic field will vary)
- Swell-induced noise, caused by induced electrical currents when conducting sea water is moving in the Earth’s magnetic field.

Previously in the project there has been an effort to suppress the noise in magnetic measurements without simultaneously suppressing target signals. This work includes:

- Suppressing geomagnetic fluctuations using measurements from a remote reference magnetometer [1, 5, 8–10]. This requires communication of raw measurement samples between different sensor locations and is hence not practical for all applications.
- Suppressing swell-induced noise using collocated pressure sensors [6, 8].
- Using linear prediction (LP) methods to whiten the noise spectrum, based on estimated noise statistics. When using 3-axial magnetometers, vector linear prediction (VLP) can be used to also exploit inter-axial statistical relationships [7, 9]. Since the statistical properties of target signals will generally be different from those of the noise, (vector) linear prediction methods will increase the signal-to-noise ratio (SNR), without requiring any remote reference sensor with accompanying communication requirements.

This report deals with target detection methods, to be used in conjunction with VLP. The ultimate objective for a target detection method would be to maximize detection probability for a given false alarm rate, based on all available knowledge of noise and target statistics. In practice, this objective will be related to the SNR of the decision variable on which a detection threshold is applied.

It is well known that each component of the observed magnetic field perturbation, when a dipole is passing by a magnetometer in a straight line, can be written as a linear combination of the three Anderson functions. In this report we propose to generate the decision variable by passing the measurements through a "generalized matched filter" (including VLP), using the Anderson functions as matched filter templates.

In 1993, a report was written at FFI on matched filtering for detection of magnetic dipole signals [2]. That report concluded that the cost in computational complexity was large compared to the gain in SNR. However, a few weaknesses in an otherwise good report spurred our interest in revisiting matched filtering detection methods:

- The matched filter templates in [2] are theoretical dipole signals for given geometries, leading to a quite large parameter space which need to be spanned by different matched filter templates. We rather propose to use orthogonal basis functions related to the Anderson functions as matched filter templates, leading to a smaller overall computational complexity.

- In [2], scalar noise whitening and matched filtering is applied to each of the three measurement axes, while we propose to also take inter-axial cross-correlations into account, leading to improved performance.

- In [2], simulated noise with $1/f$ spectral characteristics and independence between measurement axes was used. We rather use actual background noise measurements from the Herdla measurement range outside Bergen, leading to more realistic results.

3 THEORETICAL BACKGROUND

3.1 Dipole signatures and Anderson functions

It is well known that the perturbation in the magnetic field vector caused by a magnetic dipole is given by

$$\mathbf{b}(\mathbf{M},\mathbf{r}) = \frac{\mu}{4\pi}\frac{3(\mathbf{M}\cdot\mathbf{r})\mathbf{r} - r^2\mathbf{M}}{r^5} \tag{3.1}$$

where $\mathbf{M}$ is the dipole moment, $\mathbf{r}$ is the vectorial distance between the dipole and the sensor, $r = ||\mathbf{r}||$, and μ is the magnetic permeability.

If the dipole moves in a straight line with constant velocity $\mathbf{v}$, inserting $\mathbf{r}(t) = \mathbf{r}_0 + (t - t_0)\mathbf{v}$ into Eqn. (3.1) and simplifying will show that each component of $\mathbf{b}$ can be written as a linear

combination of the 3 "Anderson functions"[1]:

$$\tilde{A}_0(\tau) = \frac{1}{(1+\tau^2)^{5/2}} \tag{3.2}$$

$$\tilde{A}_1(\tau) = \frac{\tau}{(1+\tau^2)^{5/2}} \tag{3.3}$$

$$\tilde{A}_2(\tau) = \frac{\tau^2}{(1+\tau^2)^{5/2}} \tag{3.4}$$

where τ is normalized time:

$$\tau = \frac{v}{d}(t - t_0) \tag{3.5}$$

Here, t_0 is time of CPA (closest point of approach), d is CPA distance, and $v = ||\mathbf{v}||$ is speed.

The Anderson functions in their conventional form as presented above could be used as matched filter templates (basis functions) directly. To achieve better mathematical properties, the basis functions should however be orthogonalized such that $\int_{-\infty}^{\infty} A_i(\tau)A_k(\tau)dt = \delta_{ik}$ (Kronecker delta). Performing the Gram-Schmidt orthogonalization procedure on Eqns. (3.6)-(3.8), we obtain orthogonalized Anderson functions as:

$$A_0(\tau) = \frac{\sqrt{128/35\pi}}{(1+\tau^2)^{5/2}} \tag{3.6}$$

$$A_1(\tau) = \frac{\sqrt{128/5\pi}\,\tau}{(1+\tau^2)^{5/2}} \tag{3.7}$$

$$A_2(\tau) = \frac{\sqrt{56/\pi}\,(\tau^2 - 1/7)}{(1+\tau^2)^{5/2}} \tag{3.8}$$

These are the functions which are used as matched filter templates in our proposed approach.

3.2 Multi-channel generalized least squares and generalized matched filtering

Assume that a magnetic dipole is passing in a straight line near a tri-axial magnetometer, which measures the magnetic field $\mathbf{B}(t) = \mathbf{B}_0 + \mathbf{r}(t)$. Here, $\mathbf{B}_0$ is the local average (DC) value of the Earth's magnetic field, and $\mathbf{r}(t)$ is the AC-coupled measurement which is used for further processing. Let $\mathbf{n}(t)$ denote the sum of all noise sources. As discussed above, each component of the perturbation $\mathbf{b}(t)$ caused by the passing magnetic dipole can be written as a linear combination of the three orthogonalized Anderson basis functions:

$$\mathbf{r}(t) = \mathbf{b}(t) + \mathbf{n}(t) = \mathbf{C}\mathbf{a}(\tau) + \mathbf{n}(t) \tag{3.9}$$

where the matrix components are:

$$\begin{bmatrix} r_x(t) \\ r_y(t) \\ r_z(t) \end{bmatrix} = \begin{bmatrix} c_{x0} & c_{x1} & c_{x2} \\ c_{y0} & c_{y1} & c_{y2} \\ c_{z0} & c_{z1} & c_{z2} \end{bmatrix} \begin{bmatrix} A_0(\tau) \\ A_1(\tau) \\ A_2(\tau) \end{bmatrix} + \begin{bmatrix} n_x(t) \\ n_y(t) \\ n_z(t) \end{bmatrix} \tag{3.10}$$

[1]The Anderson functions are attributed to John E. Anderson, who did work in this field in the 1940's.

This model is linear in the 9 parameters c_{x0} to c_{z2}, which we call the Anderson coefficients. These are functions of the source and sensor geometry, but the exact form of these functions is irrelevant for the present discussion. Since τ and t are related through Eqn. (3.5), the model is nonlinear in the parameters v/d (time axis scaling) and t_0 (time axis shift). The shift-related nonlinearity is easily handled by implementing the processing as linear filters, and we propose to handle the scale-related nonlinearity by assuming constant value(s) of v/d.

The linearity in the Anderson coefficients is easily seen by rearranging Eqns. (3.9)-(3.10) as

$$\mathbf{r}(t) = \mathbf{A}(\tau)\mathbf{c} + \mathbf{n}(t)$$

$$= \begin{bmatrix} A_0(\tau) & A_1(\tau) & A_2(\tau) & 0 & 0 & 0 & 0 & 0 & 0 \\ 0 & 0 & 0 & A_0(\tau) & A_1(\tau) & A_2(\tau) & 0 & 0 & 0 \\ 0 & 0 & 0 & 0 & 0 & 0 & A_0(\tau) & A_1(\tau) & A_2(\tau) \end{bmatrix} \begin{bmatrix} c_{x0} \\ c_{x1} \\ c_{x2} \\ c_{y0} \\ c_{y1} \\ c_{y2} \\ c_{z0} \\ c_{z1} \\ c_{z2} \end{bmatrix} + \begin{bmatrix} n_x(t) \\ n_y(t) \\ n_z(t) \end{bmatrix} \tag{3.11}$$

and we can state the following parameter estimation problem: Given 3-axial magnetometer measurements $\mathbf{r}(t)$, estimated statistics of the noise $\mathbf{n}(t)$, and the known form of the Anderson functions, find the maximum likelihood estimates of $\mathbf{c}$, v/d, and t_0. This will actually prove difficult due to the nonlinearity in the latter two parameters, but we will show that only working with the linear parameters $\mathbf{c}$ will give a suitable decision variable for the related detection problem.

In practice, $r(t)$ will be sampled at discrete times, and the detection algorithm can be implemented as FIR (finite impulse response) digital filters. We denote the sampling interval T_s such that the sampled measurements are $r_x(kT_s)$, $r_y(kT_s)$, and $r_z(kT_s)$, for each integer k. Further, we let the input samples to the length-L FIR filter at a particular time instant be in the range $k_1 \leq k \leq k_2$, where $L = k_2 - k_1 + 1$. The input signal can hence be written

$$\mathbf{r}_{k_1:k_2} = \begin{bmatrix} \mathbf{r}_{x,k1:k2} \\ \mathbf{r}_{y,k1:k2} \\ \mathbf{r}_{z,k1:k2} \end{bmatrix} = \begin{bmatrix} r_x(k_1T_s) \\ \vdots \\ r_x(k_2T_s) \\ r_y(k_1T_s) \\ \vdots \\ r_y(k_2T_s) \\ r_z(k_1T_s) \\ \vdots \\ r_z(k_2T_s) \end{bmatrix} \tag{3.12}$$

We define the noise vector $\mathbf{n}_{k_1:k_2}$ for the sampled case in a similar manner.

The Anderson functions are also represented in discrete time as $A_{0,l} = A_0(lT_sv/d)$, $A_{1,l} = A_1(lT_sv/d)$, and $A_{2,l} = A_2(lT_sv/d)$, where l is lag in number of samples relative to the

time of CPA. We let the filter cover lags in the range $L_1 \leq l \leq L_2$ ($L_1 \geq 0$ corresponds to a causal filter), and write

$$\mathbf{A}_0 = \begin{bmatrix} A_{0,L1} \\ \vdots \\ A_{0,L2} \end{bmatrix} \qquad \mathbf{A}_1 = \begin{bmatrix} A_{1,L1} \\ \vdots \\ A_{1,L2} \end{bmatrix} \qquad \mathbf{A}_2 = \begin{bmatrix} A_{2,L1} \\ \vdots \\ A_{2,L2} \end{bmatrix} \tag{3.13}$$

$$\mathbf{A} = \begin{bmatrix} \mathbf{A}_0 & \mathbf{A}_1 & \mathbf{A}_2 & 0 & 0 & 0 & 0 & 0 & 0 \\ 0 & 0 & 0 & \mathbf{A}_0 & \mathbf{A}_1 & \mathbf{A}_2 & 0 & 0 & 0 \\ 0 & 0 & 0 & 0 & 0 & 0 & \mathbf{A}_0 & \mathbf{A}_1 & \mathbf{A}_2 \end{bmatrix} \tag{3.14}$$

With these definitions, Eqn. (3.11) can be written (for the case of sampled measurements, finite filter length, and constant v/d):

$$\mathbf{r}_{k_1:k_2} = \mathbf{A}\mathbf{c} + \mathbf{n}_{k_1:k_2} \tag{3.15}$$

3.2.1 Generalized least squares

It is known that the maximum likelihood estimate of $\mathbf{c}$ given the measurements in $\mathbf{r}$ is the *generalized least squares* (GLS) estimate,

$$\hat{\mathbf{c}}_{GLS} = (\mathbf{A}^T\boldsymbol{\Sigma}^{-1}\mathbf{A})^{-1}\mathbf{A}^T\boldsymbol{\Sigma}^{-1}\mathbf{r}_{k_1:k_2} = \mathbf{H}\mathbf{r}_{k_1:k_2} \tag{3.16}$$

where $\boldsymbol{\Sigma} = E\{\mathbf{n}\mathbf{n}^T\}$ is the noise covariance matrix (ideally known, in practice estimated from a signature-free time interval). To estimate $\mathbf{c}$ for different values of t_0, this should be recomputed for each increment of k_1 and $k_2 = k_1 + L - 1$. This can be implemented as 9 scalar FIR filters operating at each of the three components of $\mathbf{r}$ (a total of 27 different scalar FIR filters), illustrated by decomposing the matrix $\mathbf{H}$ in Eqn. (3.16) as follows:

$$\hat{\mathbf{c}}_{GLS} = \mathbf{H}\mathbf{r}_{k_1:k_2} = \begin{bmatrix} \mathbf{h}_{x0,x}^T & \mathbf{h}_{x0,y}^T & \mathbf{h}_{x0,z}^T \\ \mathbf{h}_{x1,x}^T & \mathbf{h}_{x1,y}^T & \mathbf{h}_{x1,z}^T \\ \mathbf{h}_{x2,x}^T & \mathbf{h}_{x2,y}^T & \mathbf{h}_{x2,z}^T \\ \mathbf{h}_{y0,x}^T & \mathbf{h}_{y0,y}^T & \mathbf{h}_{y0,z}^T \\ \mathbf{h}_{y1,x}^T & \mathbf{h}_{y1,y}^T & \mathbf{h}_{y1,z}^T \\ \mathbf{h}_{y2,x}^T & \mathbf{h}_{y2,y}^T & \mathbf{h}_{y2,z}^T \\ \mathbf{h}_{z0,x}^T & \mathbf{h}_{z0,y}^T & \mathbf{h}_{z0,z}^T \\ \mathbf{h}_{z1,x}^T & \mathbf{h}_{z1,y}^T & \mathbf{h}_{z1,z}^T \\ \mathbf{h}_{z2,x}^T & \mathbf{h}_{z2,y}^T & \mathbf{h}_{z2,z}^T \end{bmatrix} \begin{bmatrix} \mathbf{r}_{x,k1:k2} \\ \mathbf{r}_{y,k1:k2} \\ \mathbf{r}_{z,k1:k2} \end{bmatrix} \tag{3.17}$$

where each $\mathbf{h}$ is a column vector containing the coefficients of a length-L scalar FIR filter.

Note that the noise covariance matrix $\boldsymbol{\Sigma}$ includes the cross correlations between different measurement axes in addition to the auto-correlation in each axis:

$$\boldsymbol{\Sigma} = E\{\mathbf{n}\mathbf{n}^T\} = \begin{bmatrix} E\{\mathbf{n}_x\mathbf{n}_x^T\} & E\{\mathbf{n}_x\mathbf{n}_y^T\} & E\{\mathbf{n}_x\mathbf{n}_z^T\} \\ E\{\mathbf{n}_y\mathbf{n}_x^T\} & E\{\mathbf{n}_y\mathbf{n}_y^T\} & E\{\mathbf{n}_y\mathbf{n}_z^T\} \\ E\{\mathbf{n}_z\mathbf{n}_x^T\} & E\{\mathbf{n}_z\mathbf{n}_y^T\} & E\{\mathbf{n}_z\mathbf{n}_z^T\} \end{bmatrix} \tag{3.18}$$

It is evident that the GLS solution (3.16) is a combination of noise whitening and a modified matched filter: Premultiplication by $\mathbf{\Sigma}^{-1}$ corresponds to noise whitening. And in the case of white and uncorrelated noise ($\mathbf{\Sigma} = \mathbf{I}$), the GLS solution would collapse to the matched filter formula $\hat{\mathbf{c}} = \mathbf{A}^T\mathbf{r}$, since $\mathbf{A}^T\mathbf{A} = \mathbf{I}$ due to the orthogonalization.

3.2.2 VLP noise whitening and matched filtering

In the GLS solution, the filter lengths used for noise whitening and matched filtering are equal (both are L). This may lead to over-parameterization of the noise whitening filter (with accompanying numerical inaccuracy), as the noise process may be modelled by a relatively low-order AR process, while a long matched filter is required to capture most of the energy of the Anderson functions.

Better performance may be achieved by de-coupling the operations of noise whitening and matched filtering. We propose to use the vector linear prediction (VLP) approach discussed in [7, 9] for noise whitening[2]. The measurements $\mathbf{r}$ are passed through a multi-channel prediction error filter (PEF) $\mathbf{F}$, resulting in

$$\mathbf{r}_F = \mathbf{Fr} = \mathbf{FAc} + \mathbf{Fn} = \mathbf{A}_F\mathbf{c} + \mathbf{n}_F \tag{3.19}$$

where the subscript F indicates that the signal has been passed through the PEF. If the PEF has been properly estimated (based on noise measurements from a signature-free interval), it whitens the noise such that

$$\mathbf{\Sigma}_F = E\{\mathbf{n}_F\mathbf{n}_F^T\} \approx \mathbf{I} \tag{3.20}$$

The matrix $\mathbf{A}_F$ is obtained by passing the orthogonalized Anderson functions through the PEF. The least squares (LS) estimate for $\mathbf{c}$ given $\mathbf{r}_F$ is

$$\hat{\mathbf{c}}_{AR+LS} = (\mathbf{A}_F^T\mathbf{A}_F)^{-1}\mathbf{A}_F^T\mathbf{r}_F = (\mathbf{A}^T\mathbf{F}^T\mathbf{F}\mathbf{A}_F)^{-1}\mathbf{A}_F^T\mathbf{r}_F \tag{3.21}$$

If not interested in correctly estimating the actual parameters of $\mathbf{c}$, but rather to obtain decision variables to be thresholded, one can use the simpler alternative of disregarding the off-diagonal terms of $\mathbf{A}_F^T\mathbf{A}_F$, in which case the solution collapses to *matched filtering using the filtered Anderson functions as matched filter templates*:

$$\hat{\mathbf{c}}_{AR+MF} = [Diag(\mathbf{A}_F^T\mathbf{A}_F)]^{-1}\mathbf{A}_F^T\mathbf{r}_F \tag{3.22}$$

where the first term is a diagonal matrix which scales each component of $\hat{\mathbf{c}}$ according to the energy in the matched filter template, and premultiplication by $\mathbf{A}_F^T$ corresponds to matched filtering.

[2] [7] is classified, but the section describing the method is unclassified and has been reprinted in Appendix B for convenience

4 CASE STUDY UNDER DISTURBED CONDITIONS

4.1 Input data

To illustrate the concepts, and get an indication of the performance, we have used a case study. The case study is based on background noise measured at the Herdla measurement station in January 2006, during a campaign specifically designed to capture disturbed geomagnetic conditions. An overview of the instrumentation at Herdla can e.g. be found in [8].

Tri-axial magnetometer measurements from the Muws3P magnetometer at the main sensor platform (MSP), during the time interval Jan 23 17:52 UTC - Jan 24 01:39 UTC, are used to exemplify background noise during disturbed and varying geomagnetic conditions. The sensor is located at 25 m depth. The noise measurements are resampled to a sampling rate of 1 Hz, and passed through a 1 mHz digital highpass filter (4th order Butterworth), such that noise fluctuations in the frequency range 0.001-0.5 Hz are retained. The average value of the Earth's magnetic field, as well as very slow variations, are blocked by the filter.

Two synthetic target signals are added to the background noise. The magnetic moment of the hypothetic target vessel is 100000 Am^2 in the alongship direction, 0 in the athwartship direction, and 100000 Am^2 in the vertical direction. The vessel passes at a distance d=100 m on the west side of the sensors, with a velocity of v=3 m/s. This gives rise to a static magnetic signal with peak level of about 10 nT. The vessel passes the sensor twice in order to give two synthetic targets: In the Northward direction with CPA (closest point of approach) at 21:00 UTC, and in the Southward direction with CPA at 23:30 UTC. The target depth is equal to the sensor depth (25 m).

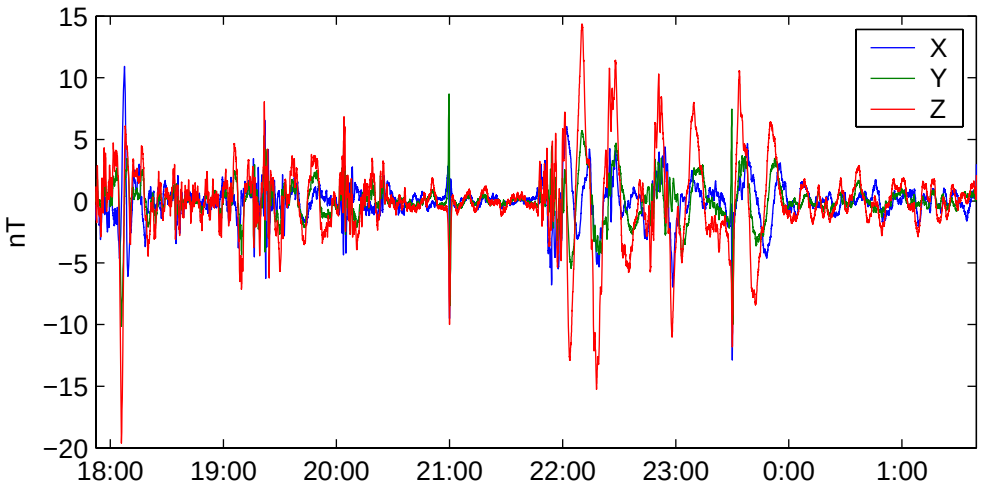

Figure 4.1 Input data to case study: Background noise collected during disturbed geomagnetic conditions, and two synthetic targets at 21:00 and 23:30.

The resulting input data, used in the subsequent analysis for the case study, is shown in Fig. 4.1. X, Y, and Z refers to the three components of the magnetic field (positive North, East, and down, respectively). Note that the background noise statistics are not stationary throughout the data set, and the time for the first target is chosen such that it clearly stands out against the

noise, while the second target is weaker than the simultaneous noise level.

4.2 Comparison of methods

Fig. 4.2 shows how the two methods presented in Sec. 3.2 performs on the case study. "AR+MF" refers to the method in Sec. 3.2.2 while "GLS" refers to the method in Sec. 3.2.1. In both cases, noise statistics estimated over the interval 18:58:58-20:22:18 (samples number 4000-9000) have been used to compute filter parameters, and the detection filter ($\mathbf{H}$ for GLS and $\mathbf{A}_F^T$ for AR+MF) has a total of 51 taps (25 precursor taps and 25 postcursor taps) at the sampling rate of 1 Hz. For the AR+MF method, a 20th order vector AR model (at the sampling rate of 1 Hz) has been used.

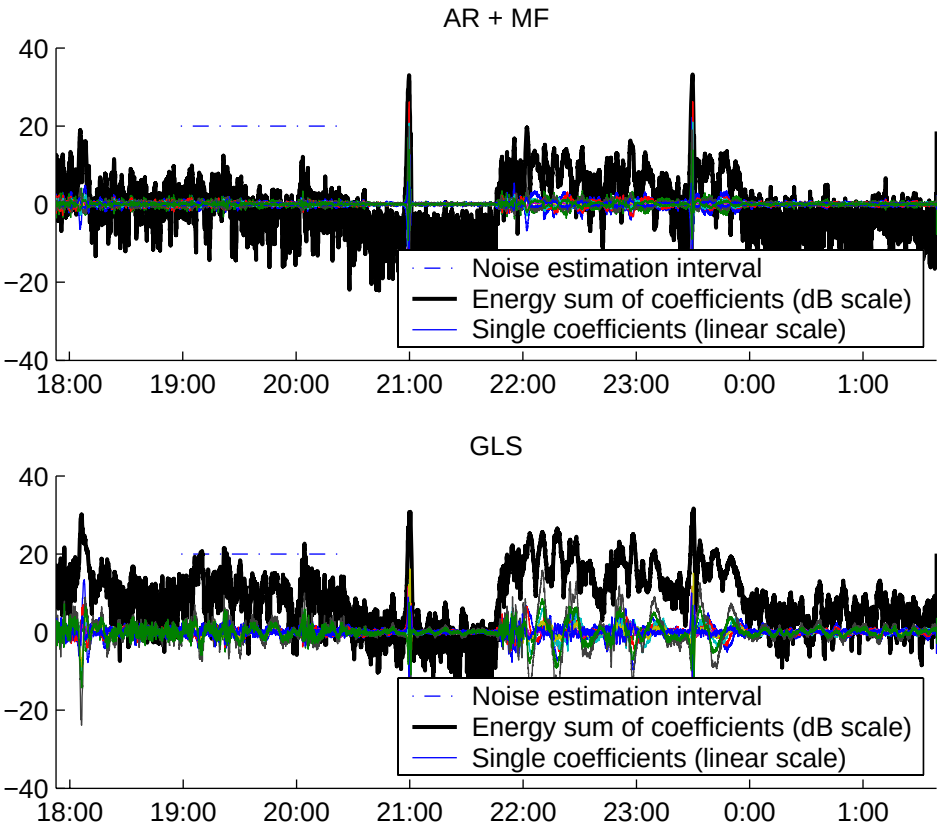

Figure 4.2 Comparison of two different methods for combined detection and noise suppression

In each case, the figure shows the nine estimated coefficients $\hat{c}_{x0}$ through $\hat{c}_{z2}$ as function of assumed CPA time t_0 as thin lines of different colours, and the energy sum of all estimated coefficients as a thick black line. The energy sum is plotted in dB units, i.e., $10\log_{10}(\hat{\mathbf{c}}^T\hat{\mathbf{c}})$.

In the input data, the target signal is about equally strong as the peak noise during the noise estimation interval. Considering the energy sum of coefficients $\hat{\mathbf{c}}^T\hat{\mathbf{c}}$ as a possible decision variable, for GLS the target signal is 8 dB above the peak noise in the noise estimation interval, while for AR+MF the same number is 21 dB.

This indicates that AR+MF in practice works better than GLS for static magnetic detection. This has also been verified for other data sets and other parameter settings. The reason for this has not been studied in detail, but a possible explanation might be that with AR+MF different filter lengths are used for noise whitening (the AR model order) and for detection, while for GLS the same filter is used for both purposes such that the noise whitening may have been over-parameterized.

In the remainder of this report, all results presented are for the AR+MF method (described in Sec. 3.2.2).

4.3 Influence of noise estimation interval

Fig. 4.3 shows the result of using another interval for noise estimation. In this case, the noise estimation interval is 21:45:38-22:52:18 (samples number 14000-18000), where the noise statistics are similar to those during the second target signal. As would be expected this gives better detection of the second target, while the noise during the previously considered noise estimation interval has increased by 6 dB compared to Fig. 4.2 above (upper plot).

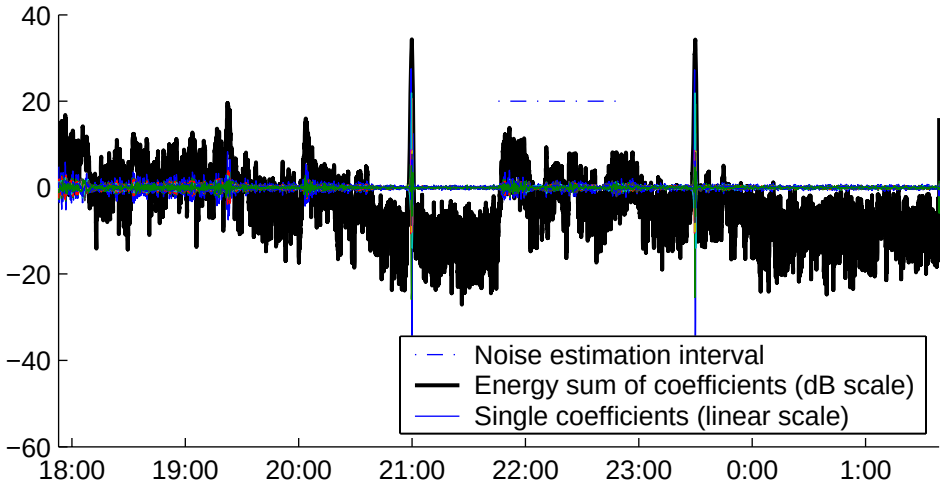

Figure 4.3 Using a different interval for noise estimation.

For optimal performance, the noise statistics should be estimated as close as possible in time to the target signal, but not include the target signal. In Sec. 5 below we show how a block-based approach can be used to achieve this in practice.

The length of the noise estimation interval should be sufficiently long to give good estimates of correlations, but not so long that the statistics are highly nonstationary during the interval or that it becomes difficult to find intervals with no signals.

4.4 Influence of bad choice of v/d

One drawback of the proposed detection method is that a value of the parameter v/d (velocity relative to range) must be chosen. This parameter basically defines the time scaling of the

signal. One approach to overcome this would be to perform the matched filtering several times, using different values of v/d. This may however not be necessary, as we find that the performance of the method is not sensitive to the choice of v/d.

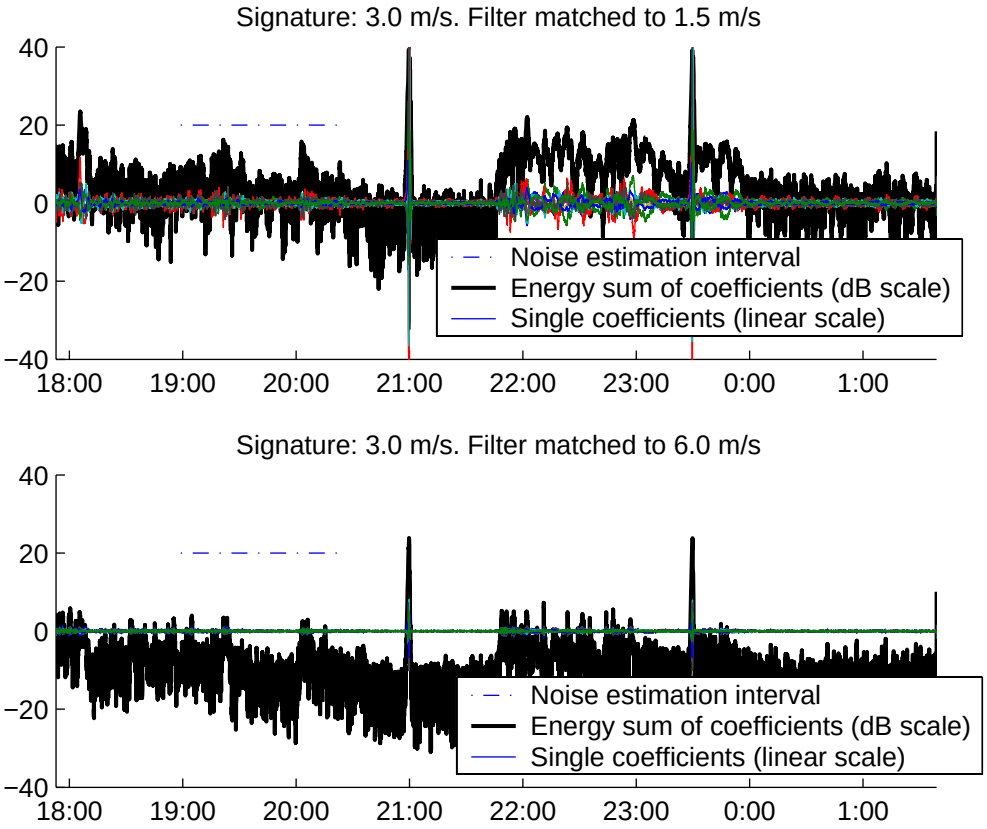

Figure 4.4 Performance when over- or under-estimating v/d by a factor of 2.

In Fig. 4.4 is shown the performance when over- or under-estimating v/d by a factor of 2. Note that the SNR of the decision variable, shown as a thick black line, is not significantly changed by this.

4.5 Noise suppression performance on single axes measurements

In Fig. 4.5 we have used the AR+MF method as above, but with independent *scalar* linear prediction and filtering on each of the three measurement axes. The resulting performance is clearly inferior to the performance using 3-axial processing (Fig. 4.2, upper plot). This suggests that when the proposed method is applied to 3-axial magnetic data, it is able to take advantage of the correlation between measurement axes in the background noise being different than in the target signals.

If a scalar magnetometer was used, the measured fluctuations would be the projection of the 3-axial fluctuations onto the Earth's field [8]. Due to the relatively high latitude, the fluctuations in the resulting measurements would be similar to the fluctuations in the Z

component. Thus, we have an indication that the proposed method would not fare particularly well in combination with a scalar magnetometer.

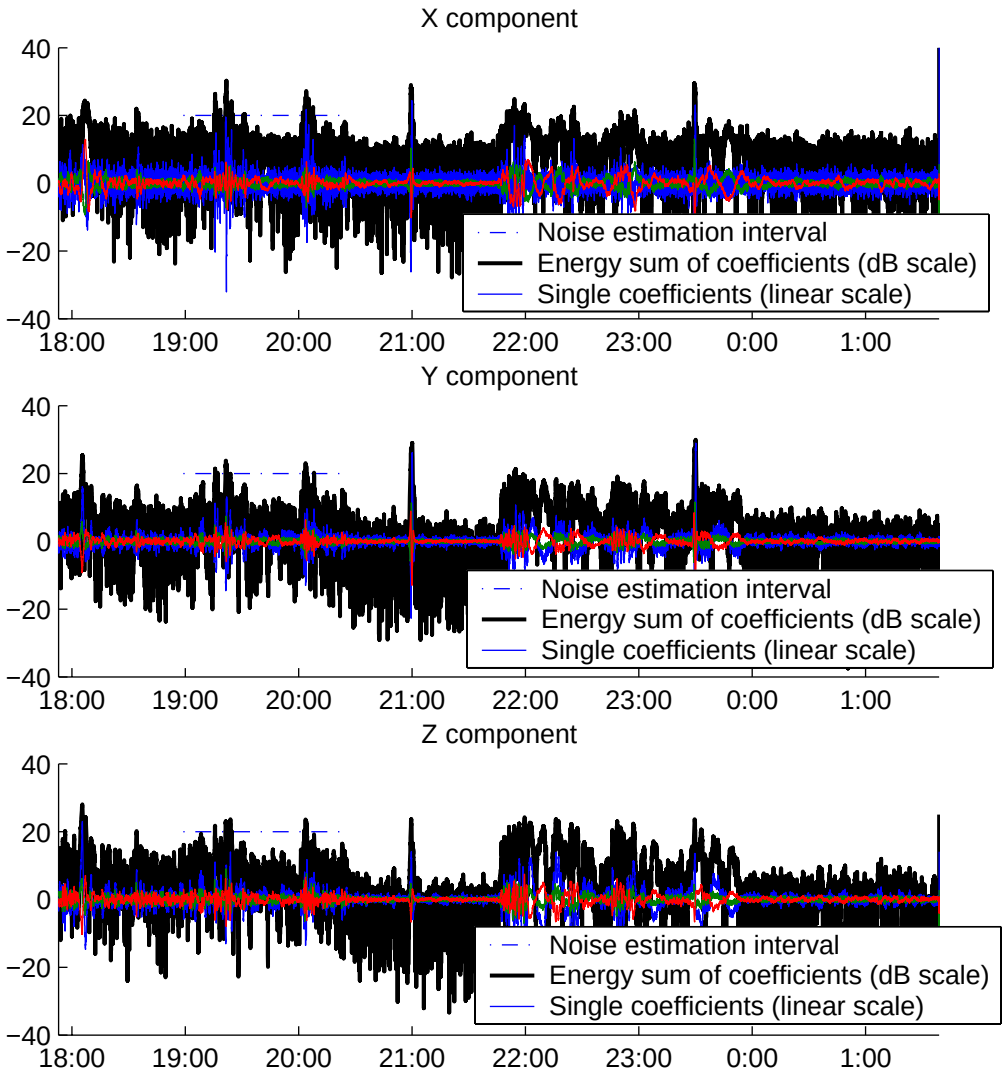

Figure 4.5 Performance when running AR+MF algorithm on single axes data.

5 BLOCK-BASED ADAPTIVE PROCESSING

5.1 Proposed algorithm

Since the statistics of geomagnetic fluctuations are non-stationary (i.e., varying with time), the vector AR model used for PEF in the “AR+MF” approach must be adapted to recent noise statistics. It is important that there are no target signals present in the interval used for noise statistics estimation, as this would lead to a filter *designed to* suppress the the target signal.

One could envision using a standard adaptive filtering procedure (see e.g. [3]) to update the AR model on a sample-by-sample basis. This, however, would suffer the following drawbacks:

(1) Any target signal would also be quickly suppressed by the adaptive PEF, unless the update rate of the adaptive filter is very slow, and (2) the matched filter $\mathbf{A}_F^T$ in Eqn. (3.22) would have to be recomputed each time the AR model is updated, i.e., at each sample interval.

We therefore rather propose using a simple block-based adaptive procedure to update the filters, with possible overlap between blocks. The procedure is readily incorporated into a buffer-based stream of input data, as shown in Fig. 5.1. The principle can be stated as follows:

- Always use filters computed from noise statistics from the last buffer where no detections were made (but not from the present buffer).
- A buffer is said to contain detection(s) if any sample of the decision variable $\hat{\mathbf{c}}^T\hat{\mathbf{c}}$ corresponding to the buffer is above a given threshold.

5.2 Performance on real noise data

To test the performance of the proposed algorithm, we have used background noise data collected at the Muws3P magnetometer at the MSP platform at Herdla, Jan. 23-24, 2006. The data is divided into eight separate files, of which we use seven[3]. The total data coverage we process is 40 hours, with geomagnetic conditions ranging from quiet to disturbed[4]. We do not see any strong vessel signals in the original data (weather conditions were harsh), but have inserted two synthetic target signals into each file. The preprocessing method (1 Hz sampling rate, 1 mHz highpass filtering) and the synthetic signals (100 m distance, 3 m/s, [100 0 100] kAm^2) are identical to the case study above, as described in Sec. 4.1. The data used in Sec. 4 is a subset of the data used below.

We have processed all the data with the same parameter settings (#samples = #seconds since sampling rate is 1 Hz):

- N_{buf}, input buffer size: 600 samples
- N_f, samples fetched into new buffer: 60 samples
- Buffer overlap, $N_{buf} - N_f$: 540 samples
- p, AR model order: 20 samples
- L_1, minimum lag of detection filter: –25 samples
- L_2, maximum lag of detection filter: 25 samples
- Total length of detection filter, $L_2 - L_1 + 1$: 51 samples
- Value of v/d assumed by detection filter: 0.03 s^{-1} (the correct value)

[3]One of the files was not used since it was quite short, and we have removed 15 minutes from the beginning of each file to ensure settling of all sensors and filters.

[4]The geomagnetic K index at Dombås was varying between 0 an 4, and in Tromsø between 0 and 6, according to the Auroral Observatory at the University of Tromsø, http://geo.phys.uit.no/yearbook/kind/

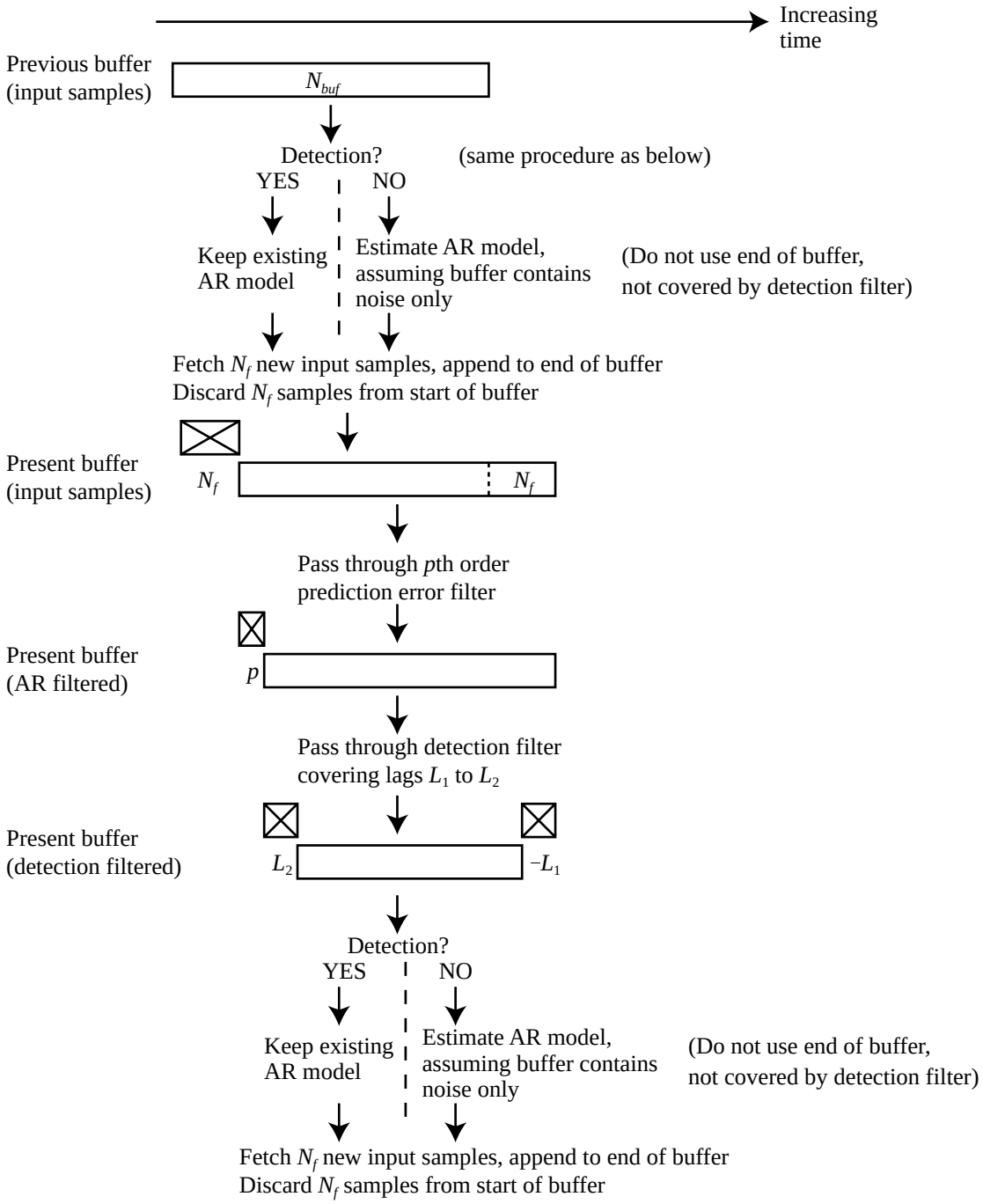

Figure 5.1 Block-adaptive processing for magnetic detection, using vector linear prediction and matched filtering to Anderson functions, "AR+MF". Symbols in italics refer to block and filter length parameters, given in number of samples.

- Samples at end of input buffer *not* used for AR model estimation: 25 samples
- Detection threshold on the decision variable $\hat{\mathbf{c}}^T\hat{\mathbf{c}}$: 28 dB

With these settings, the maximum detection delay is $N_f - L_1 = 85$ samples.

File #	Interval	Total time	Synthetic signals
1	23-Jan 08:11:06 – 23-Jan 13:20:25	5.2 hours	10:00 and 12:30
3	23-Jan 14:15:47 – 24-Jan 01:39:27	11.4 hours	21:00 and 23:30
4	24-Jan 01:56:03 – 24-Jan 05:02:50	3.1 hours	3:00 and 4:00
5	24-Jan 05:18:27 – 24-Jan 08:25:16	3.1 hours	6:00 and 8:00
6	24-Jan 08:40:48 – 24-Jan 18:36:54	9.9 hours	10:00 and 12:30
7	24-Jan 18:52:44 – 24-Jan 20:31:16	1.6 hours	19:30 and 20:00
8	24-Jan 20:48:19 – 25-Jan 02:04:18	5.3 hours	22:00 and 23:30

Table 5.1 Overview of data used to test block-based adaptive processing. All times given in UTC.

An overview of the data used to test block-based adaptive processing is shown in Tab. 5.1, and the resulting performance is shown in Fig. 5.2-5.8. It should be kept in mind that the chosen detection threshold is only 3-7 dB below the values of the decision variable corresponding to the synthetic target signals, enough for all of them to be detected but with small margins.

During files 7-8, geomagnetic conditions were very quiet, and no algorithm should have problems in discriminating between signals and noise.

During files 4-6, geomagnetic conditions were more unsettled, and the signal amplitude is approximately equal to the noise amplitude, but mostly visually distinguishable by human perception. In these cases, the proposed algorithm provides more than 15 dB discrimination between signals and noise in the decision variable.

During files 1 and 3, geomagnetic conditions were disturbed. In file 1, there are three false alarms, which do not by visual inspection look like Anderson functions. In file 3, there is one detection in addition to the synthetic signals, but it does look like Anderson functions (which the algorithm is designed to detect) and is possibly due to a passing vessel. The decision variable also comes close to the detection threshold when the noise statistics suddenly changes at approximately 22:00.

5.3 Discussion

The figures presented above correspond to one parameter combination, selected to provide adequate performance on all the data but not optimized in any sense. When testing different parameter combinations, we uncovered one drawback of the proposed algorithm, which one should be aware of: If the decision variable corresponding to a target signal does not increase above the threshold, the algorithm will assume the input buffer to contain noise only even though it does include a target signal. This will cause the filters to be designed to suppress the

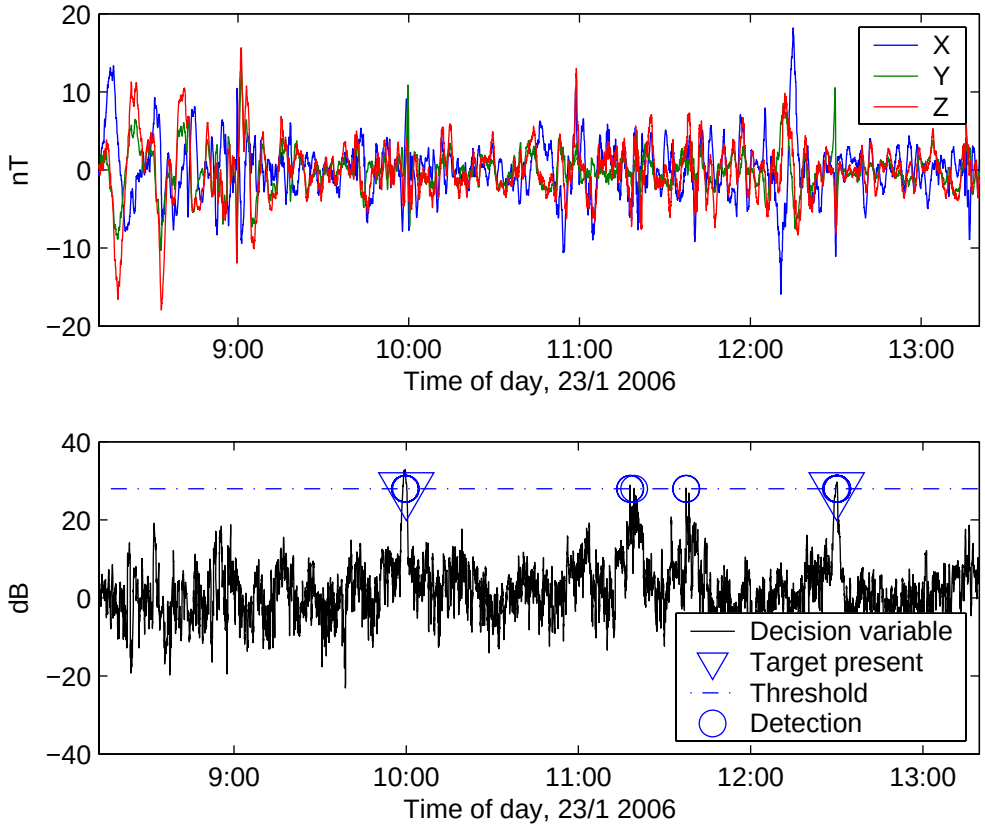

Figure 5.2 Block-based adaptive processing, file # 1. Top: Preprocessed input data with two synthetic signals. Bottom: Decision variable (last update) and detections.

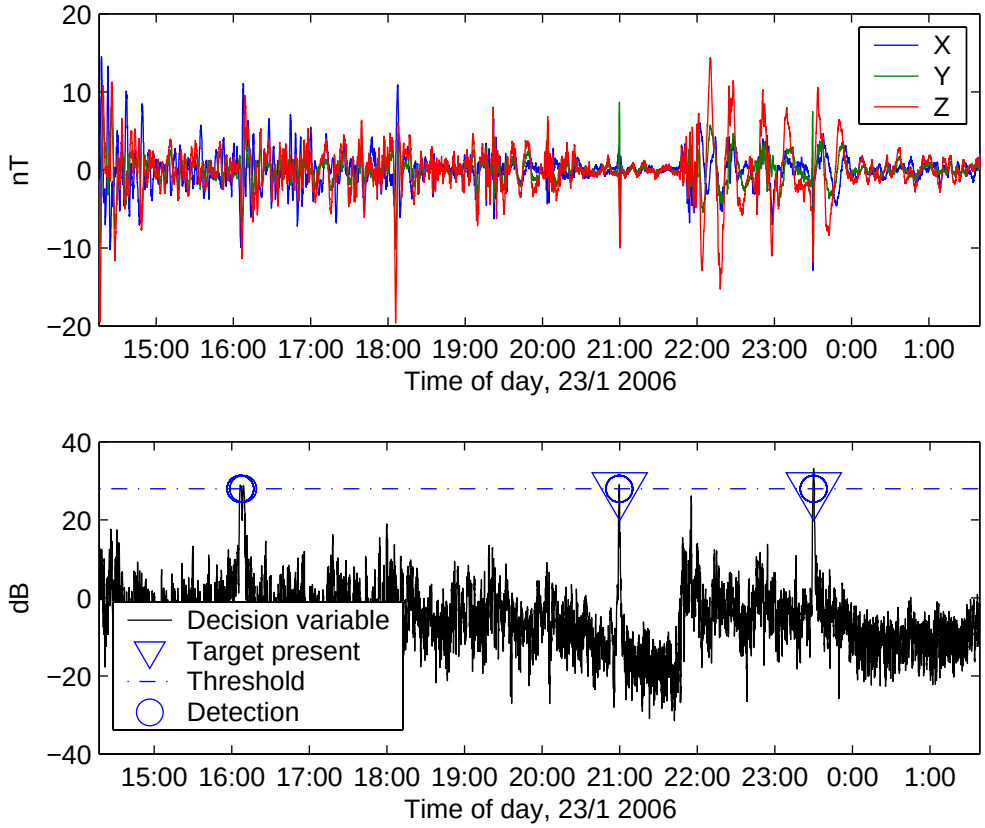

Figure 5.3 Block-based adaptive processing, file # 3. Top: Preprocessed input data with two synthetic signals. Bottom: Decision variable (last update) and detections.

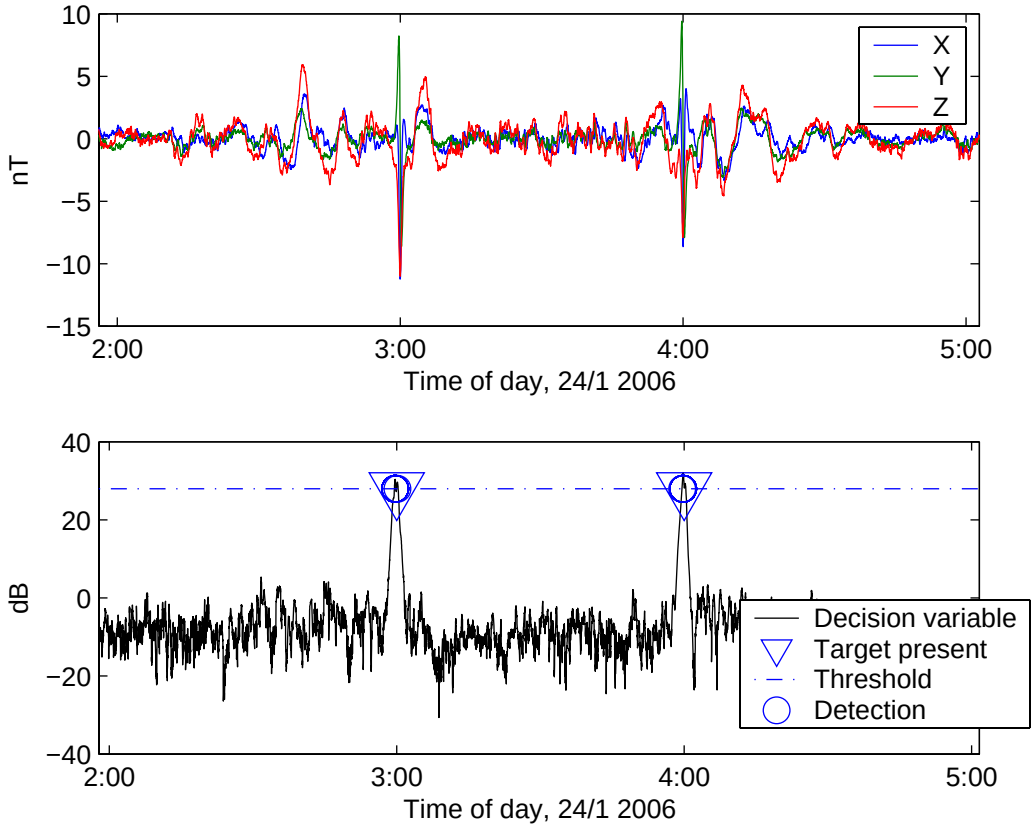

Figure 5.4 Block-based adaptive processing, file # 4. Top: Preprocessed input data with two synthetic signals. Bottom: Decision variable (last update) and detections.

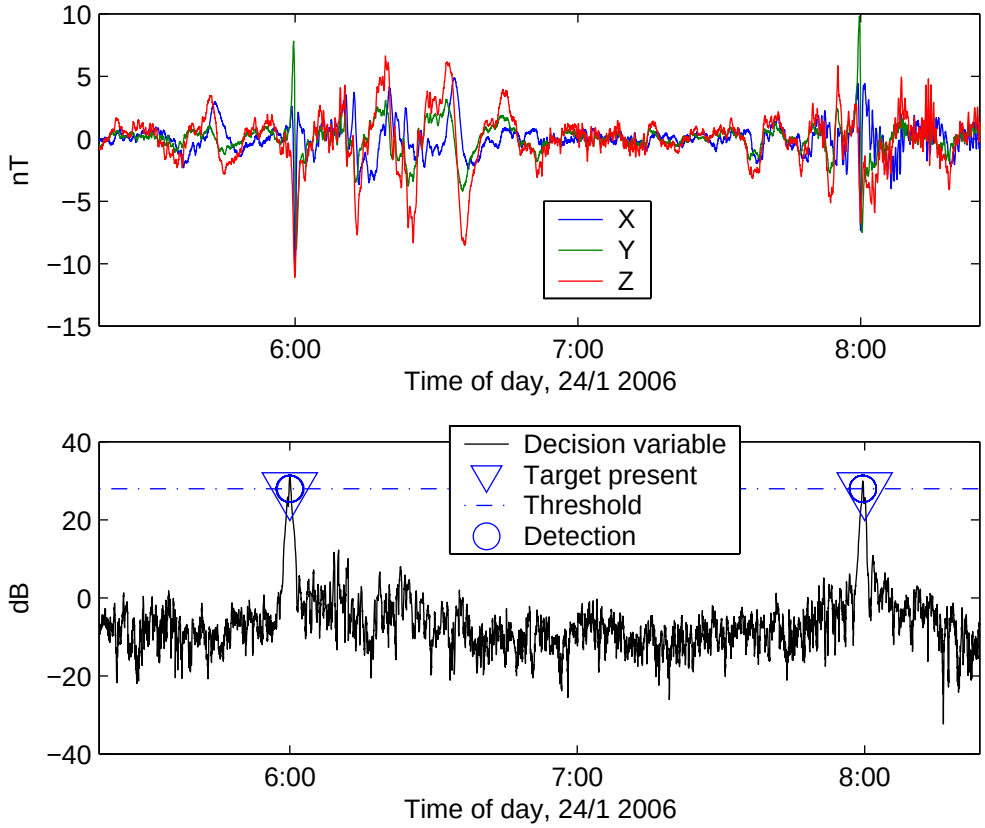

Figure 5.5 Block-based adaptive processing, file # 5. Top: Preprocessed input data with two synthetic signals. Bottom: Decision variable (last update) and detections.

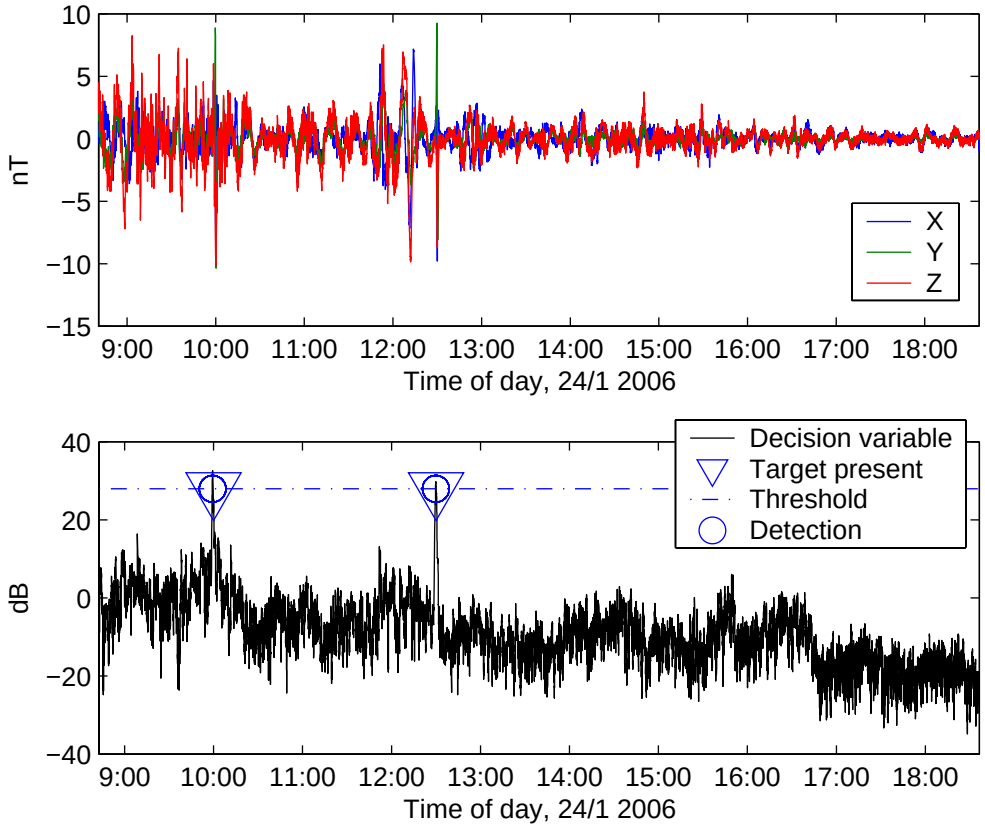

Figure 5.6 Block-based adaptive processing, file # 6. Top: Preprocessed input data with two synthetic signals. Bottom: Decision variable (last update) and detections.

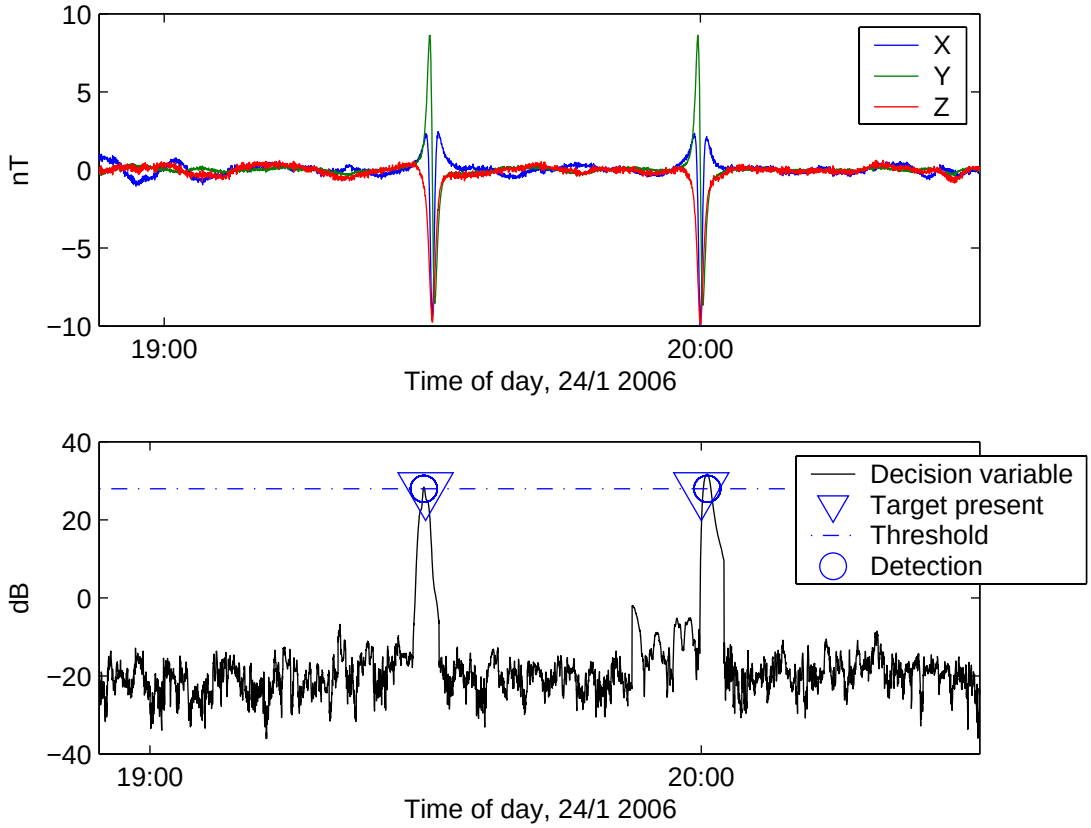

Figure 5.7 Block-based adaptive processing, file # 7. Top: Preprocessed input data with two synthetic signals. Bottom: Decision variable (last update) and detections.

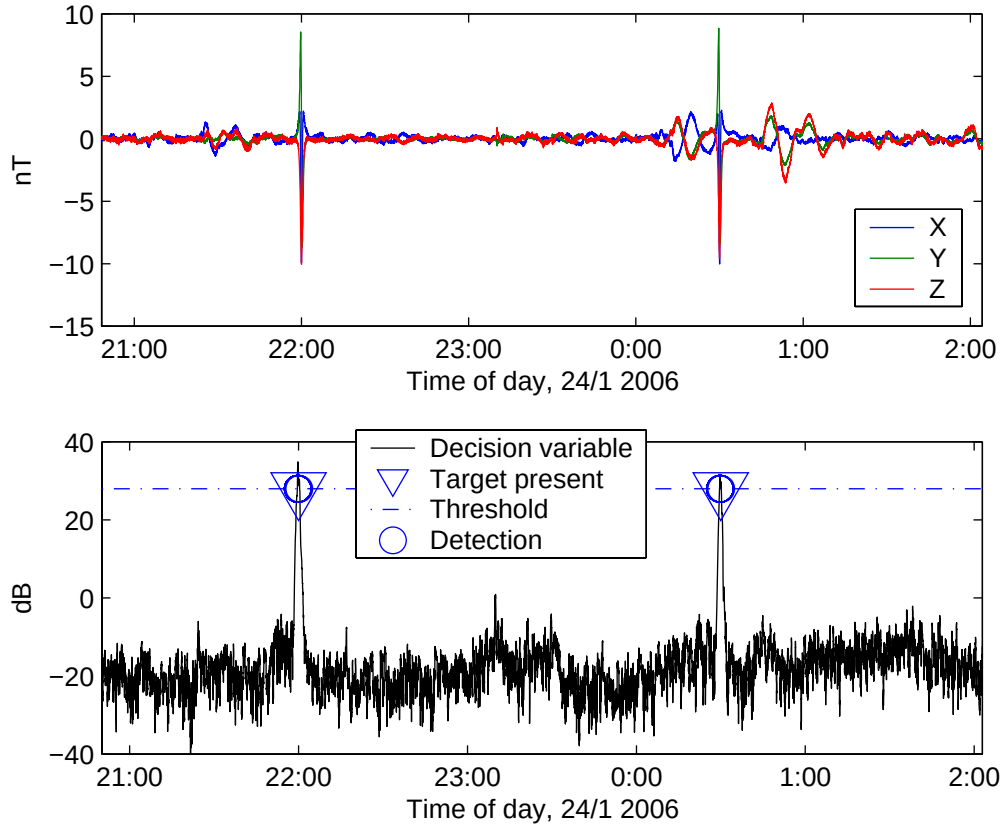

Figure 5.8 Block-based adaptive processing, file # 8. Top: Preprocessed input data with two synthetic signals. Bottom: Decision variable (last update) and detections.

target signal, which after new filters have been computed will not be visible at all in the decision variable.

We have chosen to use real noise data to demonstrate the performance. This gives realistic results, but makes it impossible to estimate false alarm rates due to the non-stationarity of the noise statistics. Therefore, ROC (receiver operating characteristics) curves are not shown in this report. One could use simulated noise data for a given level of geomagnetic activity for this purpose, e.g. using the method devised in [11]. This might, however, not be able to model inter-relationships between the X, Y, and Z axes of the geomagnetic noise, which the proposed algorithm specifically makes use of.

We have used a constant detection threshold, and not yet implemented CFAR (constant false alarm rate) processing. By CFAR is meant that the detection threshold is adapted to the noise level. When implementing CFAR processing for magnetic signals, one should be careful in the design of the CFAR update algorithm in order to handle sudden changes in noise statistics, which are relatively common in geomagnetic noise (see e.g. Fig. 5.3, at about 22:00).

If used in an area of heavy traffic, the proposed algorithm might suffer difficulty in finding intervals of data without detections. With the parameter combinations used above, 10-minute long intervals without target signals would be required on a regular basis in order to be able to update the filters.

We plan to use the proposed algorithm at sea trials in the near future, for real-time on-site assessment of the detection performance.

6 CONCLUSIONS

We have proposed a method for combined noise suppression and target detection in 3-axial magnetic measurements. Vector linear prediction is used to whiten the noise, and matched filters are used for detection. The filters are matched to the result of passing the Anderson functions through the noise whitening filters.

The filters are matched to one particular value of the parameter v/d, but are not sensitive to the actual value of v/d.

In a case study, the method has been able to extract a decision variable with an SNR of 20 dB from an input signal where the amplitude of the target signal is similar to the noise amplitude. A gain of 20 dB corresponds to increasing the detection range by a factor $\sqrt[3]{10} = 2.15$, since the amplitude of the magnetic field decreases with range as d^3, see Eqn. (3.1).

The performance of the algorithm on scalar signals is clearly inferior to its performance on 3-axial signals.

A block-based adaptive procedure for use on a buffered stream of input data has also been proposed. Good detection performance is achieved on real data, with a detection delay of 85 seconds.

References

(1) Déniel B (1997): Undersea Magnetic Noise Reduction. In *Proc. OCEANS '97*, vol 2, pages 784–788, Halifax, NS, Canada. IEEE.

(2) Grønvold B (1993): Deteksjon Av Transiente 3-Dimensjonale Vektorsignaler Med Additiv Støy. FFI/RAPPORT 93/7028, FFI, Kjeller, Norway.

(3) Haykin S (2002): *Adaptive Filter Theory*. Prentice Hall, Upper Saddle River, NJ, USA, 4th edition.

(4) Inouye Y (1983): Modeling of Multichannel Time Series and Extrapolation of Matrix-Valued Autocorrelation Sequences. *IEEE Trans. Acoustics, Speech and Signal Processing*, ASSP-31(1):45–55.

(5) Nichols E A, Morrison H F and Clarke J (1988): Signals and Noise in Measurements of Low-Frequency Geomagnetic Fields. *J. Geophys. Res.*, 93(B11):13743–13754.

(6) Otnes R (2005): Suppression of Swell Noise in Underwater Magnetic Measurements Using Collocated Pressure Sensors. In *Proc. UDT Europe 2005*, Amsterdam, Netherlands.

(7) Otnes R (2005): (U) Reducing Geomagnetic Fluctuations in Single-Sensor Magnetic Measurements Using Vector Linear Prediction. FFI/RAPPORT 2005/01644, FFI, Kjeller, Norway (CONFIDENTIAL).

(8) Otnes R (2005): Underwater Magnetic and Electric Noise Characteristics - Measurements During NGAS Trials at Herdla 2004. FFI/RAPPORT 2005/01270 (Exempt from public disclosure).

(9) Otnes R, Lucas C and Holtham P (2006): Noise Suppression Methods in Underwater Magnetic Measurements. In *Proc. Marelec 2006*, Amsterdam, Netherlands.

(10) Ridgway J (2001): Optimal MT Processing Theory for Noise Reduction in Ocean-Bottom Electromagnetic Time Series. In *Proc. Marelec 2001*, Stockholm, Sweden.

(11) Synnes S A (2005): Geomagnetic Disturbances - Power Spectrum Density as Function of Magnetic Activity Level and Latitude. FFI/NOTAT 2005/01977, FFI.

(12) Therrien C W (1992): *Discrete Random Signals and Statistical Signal Processing*. Prentice-Hall, Englewood Cliffs, NJ, USA.

(13) Wiggins R A and Robinson E A (1965): Recursive Solution to the Multichannel Filtering Problem. *J. Geophys. Res.*, 70(8):1885–1891.

APPENDIX

A ACRONYMS

AR	Auto-Regressive
CFAR	Constant False Alarm Rate
CPA	Closest Point of Approach
DRDC	Defence Research and Development Canada
FIR	Finite Impulse Response
GLS	Generalized Least Squares
JRP	Joint Research Project
MF	Matched Filter
MSP	Main Sensor Platform
NGAS	Next Generation Autonomous Sensors
NIMSES	Network Integrated Maritime Sensor Effector Systems
NURC, NATO URC	NATO Undersea Research Center
ONR	Office of Naval Research
PEF	Prediction Error Filter
ROC	Receiver Operating Characteristics
SPAWAR	Space and Naval Warfare Systems Command
SNR	Signal-to-Noise Ratio
UTC	Universal Time Coordinated
VLP	Vector Linear Prediction

B VECTOR LINEAR PREDICTION

This is an unclassified section from the classified report [7], reprinted here for convenience.

Magnetic measurements can be either scalar (total field or single axis) or vector (3-axial) signals, depending on type of magnetometer. We assume that measurements are made in discrete time using a constant sampling rate f_s.

For a real scalar signal $b(n)$, a p'th order linear predictor $\hat{b}(n)$ is nothing but a linear combination of the p previous samples:

$$\hat{b}(n) = \sum_{i=1}^{p} a_i b(n-i) \tag{B.1}$$

and the prediction error filter (PEF) describes the process of subtracting the predictor from the current sample, to obtain the "error" signal $e(n)$:

$$e(n) = b(n) - \hat{b}(n) = b(n) - \sum_{i=1}^{p} a_i b(n-i) \tag{B.2}$$

The coefficients a_i are given by the p'th order AR (autoregressive) model for the signal $b(n)$:

$$b(n) = v(n) + \sum_{i=1}^{p} a_i b(n-i) \tag{B.3}$$

where $v(n)$ is white noise, and it can be seen that $e(n)$ will be white noise provided that the AR model is correct. The AR model of a signal can be computed from the estimated autocorrelation function using the well-known Yule-Walker equations (also called normal equations), which are shown in the generalized vector case in Eq. (B.9) below.

The same concepts apply to N-dimensional vector signals ($N = 3$ for 3-axial magnetic measurements), except that the scalar AR coefficients a_i are replaced by matrices $\mathbf{A}_i$ of dimension $N \times N$ [4, 13]. This means that each component of the vector linear predictor $\hat{\mathbf{b}}(n)$ will be a linear combination of Np variables: All N components of each of the p previous sample vectors.

In the remainder of this section, we will allow all signals to be complex such that the equations are also valid for signals which have been down-converted in frequency to complex baseband[5]. We assume that the vector signal $\mathbf{b}(n)$ is organized as column vectors. The vector equivalents of eqns. (B.1)-(B.3) are then

$$\text{Linear predictor:} \qquad \hat{\mathbf{b}}(n) = \sum_{i=1}^{p} \mathbf{A}_i^H \mathbf{b}(n-i) \tag{B.4}$$

$$\text{PEF:} \qquad \mathbf{e}(n) = \mathbf{b}(n) - \hat{\mathbf{b}}(n) = \mathbf{b}(n) - \sum_{i=1}^{p} \mathbf{A}_i^H \mathbf{b}(n-i) \tag{B.5}$$

$$\text{AR model:} \qquad \mathbf{b}(n) = \mathbf{v}(n) + \sum_{i=1}^{p} \mathbf{A}_i^H \mathbf{b}(n-i) \tag{B.6}$$

The autocorrelation function (ACF) of a vector signal will be a $N \times N$ matrix-valued function of lag l:

$$\mathbf{R}_{\mathbf{b}}(l) = E\{\mathbf{b}(n)\mathbf{b}^H(n-l)\} \tag{B.7}$$

and can be estimated empirically from L consecutive sample vectors as[6]

$$\hat{\mathbf{R}}_{\mathbf{b}}(l) = \frac{1}{L} \sum_{n=l+1}^{L} \mathbf{b}(n)\mathbf{b}^H(n-l), \qquad l \geq 0 \tag{B.8}$$

Note that we have the conjugate symmetric property $\mathbf{R}_{\mathbf{b}}(-l) = \mathbf{R}_{\mathbf{b}}^H(l)$ and $\hat{\mathbf{R}}_{\mathbf{b}}(-l) = \hat{\mathbf{R}}_{\mathbf{b}}^H(l)$.

The p'th order AR model of a vector signal can be estimated by solving the Yule-Walker equations, which for this generalized case can be written

$$\begin{bmatrix} \hat{\mathbf{R}}_{\mathbf{b}}(0) & \hat{\mathbf{R}}_{\mathbf{b}}(1) & \cdots & \hat{\mathbf{R}}_{\mathbf{b}}(p-1) \\ \hat{\mathbf{R}}_{\mathbf{b}}(-1) & \hat{\mathbf{R}}_{\mathbf{b}}(0) & & \vdots \\ \vdots & & \ddots & \\ \hat{\mathbf{R}}_{\mathbf{b}}(-(p-1)) & \cdots & & \hat{\mathbf{R}}_{\mathbf{b}}(0) \end{bmatrix} \begin{bmatrix} \mathbf{A}_1 \\ \mathbf{A}_2 \\ \vdots \\ \mathbf{A}_p \end{bmatrix} = \begin{bmatrix} \hat{\mathbf{R}}(-1) \\ \hat{\mathbf{R}}(-2) \\ \vdots \\ \hat{\mathbf{R}}(-p) \end{bmatrix} \tag{B.9}$$

[5] Note, however, that we only process real-valued signals in the experimental part of this report.

[6] This is the biased estimate of the ACF, which has better mathematical properties than the unbiased estimate obtained by normalizing by $L - l$ rather than by L [12].

Each element in (B.9) is an $N \times N$ matrix, and the overall matrix equation can be interpreted as N scalar equation sets (one for each column of the right hand side), each containing Np equations in Np unknowns, such that the total number of scalar unknowns is N^2p.

In the present study we have solved these equations directly by Gaussian elimination using Matlab. If computational complexity becomes an issue, the equations can be solved more efficiently by recursive methods exploiting the block Toeplitz structure. For the scalar case, several such methods exist [12], named after Levinson/Durbin, Schur, and Burg. The Levinson/Durbin and Burg methods have been generalized to the vector case in [4, 13].